Dynamic amplification of extreme precipitation sensitivity

Ji Nie[a,1], Adam H. Sobel[b,c], Daniel A. Shaevitz[c], and Shuguang Wang[c]

[a]Department of Atmospheric and Oceanic Sciences, Peking University, Beijing 100871, China; [b]Lamont–Doherty Earth Observatory, Columbia University, Palisades, NY 10964; and [c]Department of Applied Physics and Applied Mathematics, Columbia University, New York, NY 10027

Edited by Kerry A. Emanuel, Massachusetts Institute of Technology, Cambridge, MA, and approved July 27, 2018 (received for review January 11, 2018)

A useful starting hypothesis for predictions of changes in precipitation extremes with climate is that those extremes increase at the same rate as atmospheric moisture does, which is $\sim 7\%\ K^{-1}$ following the Clausius–Clapeyron (CC) relation. This hypothesis, however, neglects potential changes in the strengths of atmospheric circulations associated with precipitation extremes. As increased moisture leads to increased precipitation, the increased latent heating may lead to stronger large-scale ascent and thus, additional increase in precipitation, leading to a super-CC scaling. This study investigates this possibility in the context of the 2015 Texas extreme precipitation event using the Column Quasi-Geostrophic (CQG) method. Analogs to this event are simulated in different climatic conditions with varying surface temperature (T_s) given the same adiabatic quasigeostrophic forcing. Precipitation in these events exhibits super-CC scaling due to the dynamic contribution associated with increasing ascent due to increased latent heating, an increase with importance that increases with T_s. The thermodynamic contribution (attributable to increasing water vapor; assuming no change in vertical motion) approximately follows CC as expected, while vertical structure changes of moisture and diabatic heating lead to negative but secondary contributions to the sensitivity, reducing the rate of increase.

extreme precipitation | convection | climate change

How will precipitation extremes respond to climate change? As climate warms, the water vapor content of a saturated air column increases with surface temperature (T_s) at a rate of $\sim 7\%\ K^{-1}$ following the Clausius–Clapeyron (CC) relation (1, 2), and the actual water vapor content increases similarly in both models and observations (3, 4). The response of global mean precipitation to warming is largely constrained by global energy balance ($\sim 2\%\ K^{-1}$) (3), while regional mean precipitation increases more variably (5). Observations of precipitation extremes, however, show that they increase more rapidly than the regional mean precipitation does in most regions, increasing even where the mean precipitation decreases, albeit with significant variability across geographic locations (6, 7). General circulation models (GCMs) project that, in midlatitudes, the rate at which precipitation extremes increase is close to CC scaling. In the tropics, some models project super-CC scaling, although with considerable intermodel spread (8–11). Given that GCMs poorly represent many characteristics of precipitation extremes in the current climate, such as their climatology (8) and dependences on temperature on the interannual timescale (12), it is appropriate to view their predictions of changes in precipitation extremes with warming with a critical eye. Simulations in regional climate models with finer horizontal resolutions usually show greater sensitivity of extreme precipitation to warming than do GCM simulations (13–19), suggesting that GCMs may underestimate this sensitivity.

By separating the sensitivity of precipitation extremes to surface temperature into a thermodynamic component—that due to the increase of atmospheric moisture with temperature (i.e., that which leads to CC scaling)—and a dynamic component, which is the change of large-scale vertical motion (1), most of the uncertainty in extreme precipitation sensitivity comes from the dynamic component (9, 10). It is suggested that the increased latent heating associated with increased precipitation may further modify the atmospheric circulations associated with extreme precipitation events, changing both the magnitude and vertical structure of their large-scale vertical motion and resulting in a feedback between the thermodynamic and dynamic components (2, 20). This feedback may be either positive or negative and is key to explaining the wide spread of extreme precipitation sensitivity in GCM simulations (9, 10) and the regional distribution of extreme precipitation sensitivity in observations (6, 7).

In this paper, we investigate the sensitivity of extreme precipitation to warming using the idealized Column Quasi-Geostrophic (CQG) modeling framework (21, 22). This framework allows for a relatively clean mechanistic interpretation of the feedbacks between the thermodynamic and dynamic contributions to extreme precipitation events. CQG extends the notion of parameterization of large-scale dynamics (23–26) from the tropics to the extratropics. In the tropics, large-scale vertical motion is almost entirely controlled by diabatic heating, while in the extratropics, dry adiabatic balanced potential vorticity (PV) dynamics also plays an important role in generating large-scale vertical motion. CQG allows interaction between large-scale vertical motion and convection in a limited domain, thus distinguishing this study from previous cloud-resolving model (CRM) studies that have examined extreme precipitation sensitivity under Radiative–Convective Equilibrium with no large-scale vertical motion (27).

Significance

Changes in precipitation extremes under climate change are subject to substantial uncertainty. Atmospheric moisture increases alone would make extreme rain events heavier at a well-understood rate of $\sim 7\%\ K^{-1}$, but a component associated with storm dynamics is much less well-understood and can either amplify or reduce that moisture-driven intensification. This paper uses an idealized modeling framework to understand the coupling of these two components, simulating one actual heavy rain event in both the present climate and hypothetical perturbed climates. The increased heating due to increased moisture drives a dynamical increase in large-scale ascent, amplifying the moisture-driven response by as much as a factor of two for warmer climates.

Author contributions: J.N. and A.H.S. designed research; J.N. performed and analyzed numerical simulations; J.N. and D.A.S. analyzed reanalysis data; and J.N. wrote the paper with contributions from A.H.S., D.A.S., and S.W.

The authors declare no conflict of interest.

This article is a PNAS Direct Submission.

[1]To whom correspondence should be addressed. Email: jinie@pku.edu.cn.

This article contains supporting information online at www.pnas.org/lookup/suppl/doi:10.1073/pnas.1800357115/-/DCSupplemental.

The experiments here are designed based on an extreme precipitation event occurring in May 2015 over the southcentral United States. We choose a specific observed event so that we can use a realistic synoptic forcing, derived from reanalysis, and validate our method by comparing model results with observations. We argue, however, that our results have implications for other extreme events with broadly similar characteristics. We simulate the 2015 event under a wide range of T_s with the same large-scale Quasi-Geostrophic (QG) adiabatic forcings obtained from reanalysis data. This approach is conditioned on the large-scale perturbations and considers the sensitivity only due to the slowly varying thermodynamic component of the climate—namely, the background temperature (T) and moisture (q)—thus being similar to event-based "highly conditional," "pseudoglobal warming," or "storyline" event attribution studies (16, 19, 28–32). We show that the positive feedback between the thermodynamic and dynamic components of the extreme precipitation sensitivity can be straightforwardly understood and quantified under CQG, thus providing a theoretical estimate of the extreme precipitation sensitivity that may be a useful complement to those from GCMs. A limitation is that, due to our focus on a single event and assumed constancy of F, no statement can be made about changes in the probability of occurrence of an event of this type.

Methods

Our implementation of CQG uses a CRM, here the System for Atmospheric Modeling (33), to explicitly resolve small-scale convection in a limited domain. As in our previous studies (21, 22), we parameterize the large-scale vertical motion using the single-wavenumber (k) QG ω equation:

$$\partial_{pp}\omega - \sigma\left(\frac{k}{f_0}\right)^2\omega = -\frac{1}{f_0}\partial_p Adv_\zeta + \frac{R}{p}\left(\frac{k}{f_0}\right)^2 Adv_T + \frac{R}{p}\left(\frac{k}{f_0}\right)^2 Q. \quad [1]$$

ω is pressure-coordinate vertical velocity, σ is dry static stability, f_0 is the Coriolis parameter, and Q is diabatic heating (here computed explicitly by the CRM). Adv_ζ and Adv_T are the large-scale horizontal advections of absolute vorticity and temperature, respectively. The first two right-hand side (RHS) terms represent the adiabatic QG forcing (F) (34), while the last RHS term represents the effects of the diabatic heating on ω. After each CRM time step, the large-scale ω is diagnosed with Eq. **1**; then, the vertical advection of T and q associated with ω are applied on the CRM domain, thus coupling convection and large-scale dynamics. Comparing with conventional CRM simulations in which ω is prescribed, in CQG, we only need to prescribe F, while convection, precipitation, and ω are simulated interactively. Additional details of the model and experiments are in *SI Appendix*.

Numerical simulations are based on the extreme precipitation event occurring in Texas and Oklahoma during May 22–26, 2015. Meteorological variables from the European Center for Medium-Range Weather Forecasting's interim reanalysis (35) are used in this study both to force the CRM and as a reference against which to compare the simulations. Based on the rainfall distribution associated with the event, we define a latitude–longitude box (Fig. 1) as the target region from which data are extracted for deriving F and where modeled precipitation is compared with observations.

The experiments consist of a control case and a series of perturbed cases. The objective in the control case is to reproduce the extreme precipitation that was observed under the current climate in the actual event, while the perturbed cases aim to simulate precipitation from events with the same synoptic forcing in climates with varying background T and q profiles that depend on T_s in a systematic way. The perturbed cases are constructed with the help of the Coupled Model Intercomparison Project (CMIP5) simulations (*SI Appendix*). In each case, the model is forced with the same large-scale adiabatic QG forcings and the large-scale horizontal moisture advection (Adv_q) (*SI Appendix*, Fig. S2) taken from the reanalysis to isolate the dependence of extreme precipitation on background conditions. This implies an underlying hypothesis that changes in thermodynamic environment will dominate changes in synoptic-scale PV dynamics in determining changes in precipitation extremes with warming. We view this as a plausible starting hypothesis given the much larger uncertainties in circulation changes compared with thermodynamic changes (37).

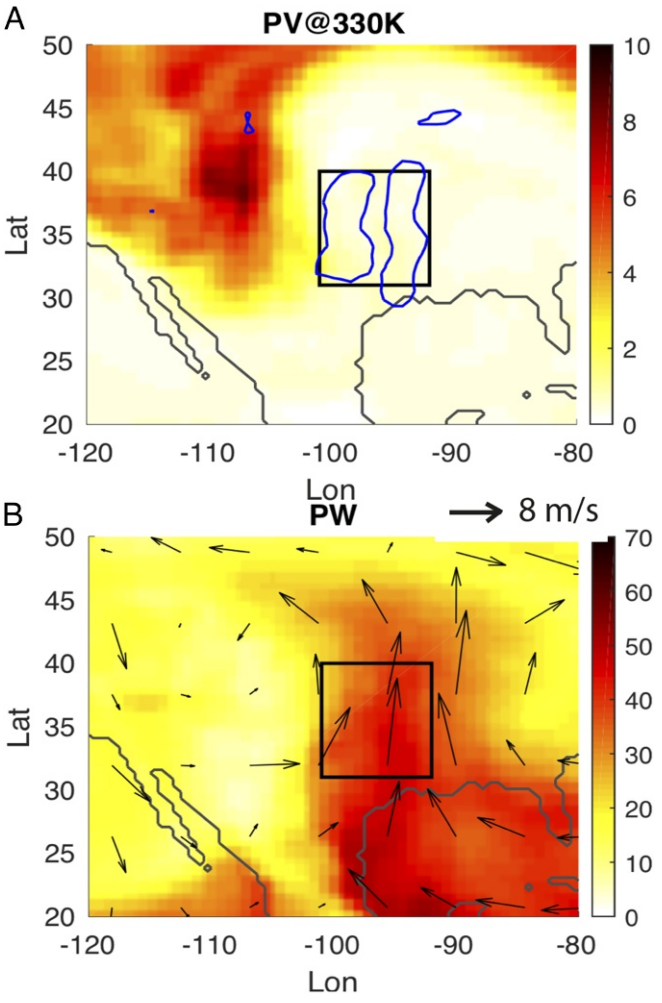

Fig. 1. (*A*) Ertel PV (in PV units; color) on the 330 K isentropic surface on May 24 and areas (blue contours) where the cumulative precipitation [Climate Prediction Center precipitation data (36)] between May 22 and May 26 was greater than 50 mm. (*B*) Precipitable water (PW; color) and the 850-hPa horizontal winds (black arrows) on May 24. The black rectangles indicate the regional box (101°W ~ 92°W and 31°N ~ 40°N) within which most of the rain during the 2015 event fell.

Results

Preceded by several days of heavy rain, a slowly propagating storm led to even heavier precipitation across Texas and Oklahoma during May 24–26, 2015 (Fig. 2*A*), causing record-breaking floods. This extreme event was caused by a strong upper level PV intrusion from higher latitudes to the west of the precipitating region (Fig. 1*A*). Associated with the PV tongue was a low-pressure trough extending down to the lower troposphere. Correspondingly, a lower level southerly jet brought very humid air from the Gulf of Mexico to the precipitating region (Fig. 1*B*). The advection of the upper level PV anomalies induced ascending motion in the free troposphere, reducing free tropospheric stability and encouraging convection. This event produced one of the largest 5-d cumulative precipitation totals for the box of interest during the period 1948–2015, causing May of 2015 to be the wettest month among all Mays in the record (*SI Appendix*, Fig. S1).

The simulated precipitation using CQG in the control case matches the observed precipitation series reasonably well (Fig. 2*A*). It reproduces the maximum in rainfall around May 24 and other minor peaks mostly within the range of ERA reanalysis and observed precipitation. The time evolution of QG ω in the

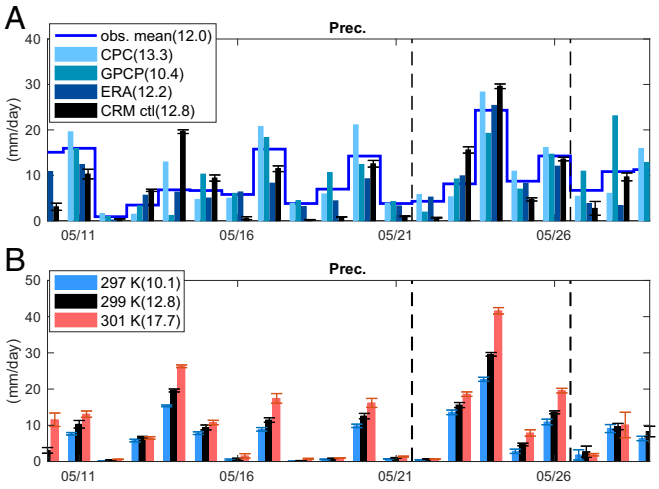

Fig. 2. (*A*) Daily precipitation from the Climate Prediction Center (CPC) data, the Global Precipitation Climatology Project (GPCP) precipitation data (38), ERA reanalysis (12-h reforecast), and CRM simulation of the control case. The blue line is the mean of the three observations and reanalysis dataset. (*B*) Daily precipitation of the control case and two perturbed cases. Error bars indicate the SD among six ensemble members, which are different realizations with small random noise in the initial conditions (*SI Appendix*). Numbers in brackets are the mean precipitation between May 22 and 26 (marked by the black vertical dash lines).

simulation also matches the reanalysis reasonably well (*SI Appendix*, Fig. S3). The precipitation comparisons between the control and perturbed cases show the sensitivity of the precipitation to the background climate. As an example, Fig. 2*B* shows daily precipitation from the control case ($T_s = 299$ K), the $T_s = 297$ K case, and the $T_s = 301$ K case. Each case includes six ensemble members with different realizations of small random noise in the initial conditions (*SI Appendix*). Precipitation increases with warming strongly and far above the variability within the ensemble. We focus on the 5-d mean precipitation between May 22 and May 26, 2015 (denoted P) hereafter. Precipitation totals on this timescale are relevant to impacts on larger scales (e.g., flooding in large river basins) and also relevant to interpretations of GCM results often used in the context of climate change studies. Many previous studies have used high-resolution regional simulations to examine changes with warming of convective-scale precipitation and updrafts (13, 15–19), which are of great societal relevance to local areas (39). Analyses of convective-scale responses to the surface warming are presented in *SI Appendix* as a complement to our primary focus on the larger space and timescale.

As T_s increases from 293 K to 305 K, P increases exponentially from 7.4 to 36.3 mm/d (Fig. 3*A*). We calculate the exponential growth rate locally at each T_s ($\frac{\delta \ln P}{\delta T_s}$ using centered differences, except for the first and last values, in which forward and backward differences are used) (Fig. 3*B*). The precipitation sensitivity to surface temperature, $\frac{\delta \ln P}{\delta T_s}$, is not constant but increases from 7% K^{-1} at $T_s = 293$ K to 17% K^{-1} at $T_s = 301$ K; then, it remains roughly constant as T_s further increases. Overall, the extreme precipitation sensitivity substantially exceeds CC scaling, implying an important role for dynamic feedbacks. The results here are qualitatively consistent with the super-CC scaling of extreme precipitation found in observations on the interannual timescale (12) and in some numerical modeling studies (10, 14, 16).

We apply the conventional decomposition (10) to quantify the thermodynamic and dynamic components of the extreme precipitation sensitivity. This decomposition is based on the

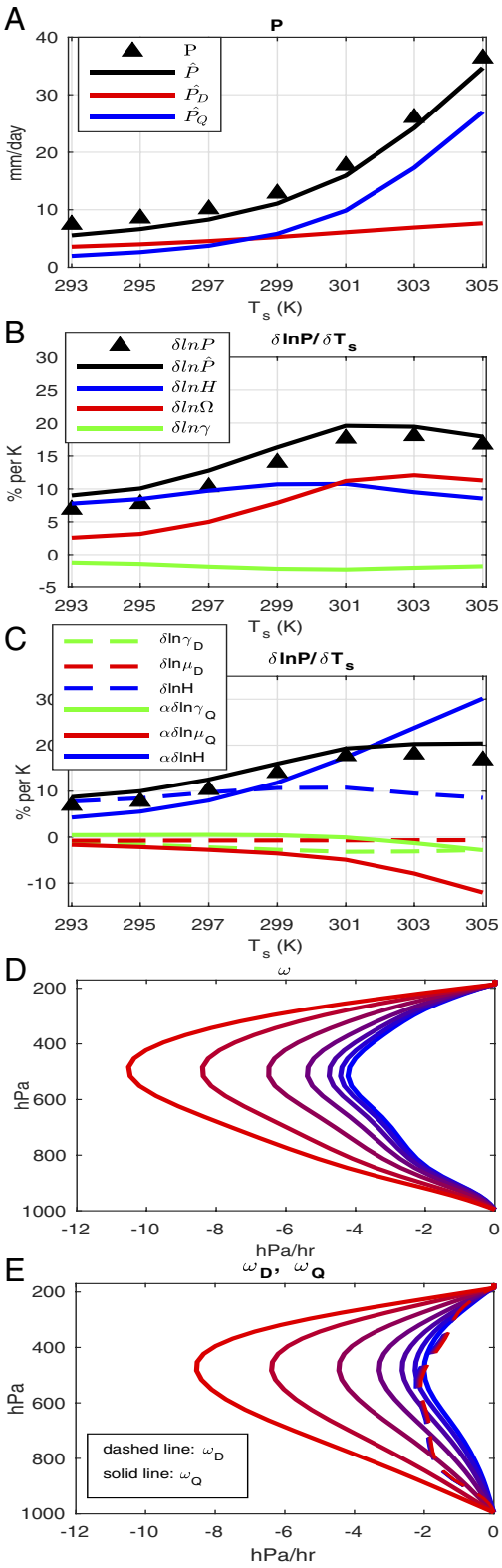

Fig. 3. (*A*) P, $\hat{P}$, $\hat{P_D}$, and $\hat{P_Q}$ as functions of T_s. *B* and *C* are the decompositions of $\frac{\delta \ln P}{\delta T_s}$ based on Eqs. **3** and **5**, respectively. The black solid lines show the sum of the color lines. *D* and *E* show ω, ω_D, and ω_Q. The changing of the line colors from blue to red corresponds to cases in which T_s increases from 293 to 305 K. Note that the dashed lines in *E* almost all collapse to the same line.

approximation that heavy precipitation comes primarily from the vertical advection of moisture: $P \approx \hat{P} \equiv -\langle \omega \partial_p q \rangle$ ($\langle * \rangle = \frac{1}{g}\int * dp$ denotes pressure vertical integration), an approximation supported by our budget analysis (*SI Appendix*, Fig. S4). $\hat{P}$ is only slightly smaller than P (Fig. 3*A*), and $\frac{\delta \ln \hat{P}}{\delta T_s}$ is only slightly greater than $\frac{\delta \ln P}{\delta T_s}$ (Fig. 3*B*) ($\delta \ln P \approx \frac{\hat{P}}{P}\delta \ln \hat{P}$). Since the approximation $\hat{P} \approx P$ holds well and at the same time, simplifies interpretation, from here on, we focus on $\delta \ln \hat{P}$. By separating the amplitudes and vertical structures of ω and $\partial_p q$, we have

$$\hat{P} = \gamma H \Omega, \qquad [2]$$

where Ω is the absolute value of ω at 500 hPa, a metric of vertical motion amplitude in middle troposphere, and $H = \langle q \rangle$ is column precipitable water. The parameter $\gamma = -\langle \frac{w}{\Omega} \frac{\partial_p q}{H} \rangle$ absorbs the covariances of the vertical structures of normalized vertical velocity ($\frac{w}{\Omega}$) and normalized moisture stratification ($\frac{\partial_p q}{H}$). The percentage changes of $\hat{P}$ can thus be written as

$$\delta \ln \hat{P} = \delta \ln H + \delta \ln \Omega + \delta \ln \gamma. \qquad [3]$$

The RHS terms are the thermodynamic component, the dynamic component, and a component due to changes in the vertical structures of ω and q, respectively.

The results of the decomposition in Eq. **3** are shown in Fig. 3*B*. $\delta \ln H$ varies little over all cases, with a mean value of $9\%\ \mathrm{K}^{-1}$. This value is slightly higher than the CC scaling, because the upper troposphere warms more than the surface does (*SI Appendix*, Fig. S6*B*) and the precipitable water increases faster than the surface water vapor with T_s (27, 40). The changes in covariance of vertical structure are small and negative ($\delta \ln \gamma \approx -2\%\ \mathrm{K}^{-1}$). The dynamic component, $\delta \ln \Omega$, is positive and contributes significantly to the super-CC scaling, consistent with the increases of ω with T_s (Fig. 3*D*). Interestingly, unlike the other two terms that are nearly independent of T_s, $\delta \ln \Omega$ increases from 2.5 to $11\%\ \mathrm{K}^{-1}$ and then remains constant, explaining most of the dependence of $\delta \ln \hat{P}$ on T_s.

Next, we look into the dynamic component ($\delta \ln \Omega$). Given the linearity of the QG ω equation (Eq. **1**), we can separate ω as $\omega = \omega_D + \omega_Q$, in which ω_D is the part due to the imposed dry adiabatic dynamic forcing (F), while ω_Q is due to diabatic heating (Q). ω_D and ω_Q can be calculated by solving Eq. **1**, including the first two terms on the RHS and then, the third term on the RHS. The comparison of the ω components in the control case between results from the reanalysis and those from the simulation again shows reasonable agreement (*SI Appendix*, Fig. S3). By examining the perturbed cases, we see that ω_D remains almost unchanged. This is largely due to the fact that the adiabatic dynamic forcing F is prescribed to be fixed in experiment design. The increases of ω are mostly due to the increases of ω_Q (Fig. 3*E*).

In our calculations, σ is evaluated from the instantaneous horizontal-averaged temperature profile in the CRM simulations and increases with warming (the so-called lapse rate effect). However, the change of σ is relatively small here so that the resulting decreases in ω_D are similarly small. The increases in σ also partly compensate for increases in diabatic heating, but its changes are sufficiently small, and the heating changes dominate the response.

The extreme precipitation sensitivity can be decomposed based on the QG ω separation. Defining $\hat{P_D} \equiv -\langle \omega_D \partial_p q \rangle$ and $\hat{P_Q} \equiv -\langle \omega_Q \partial_p q \rangle$ as precipitation due to vertical moisture advection by ω_D and ω_Q, respectively, we have

$$\hat{P} = \hat{P_D} + \hat{P_Q} = (1+\alpha)\hat{P_D}, \qquad [4]$$

where $\alpha = \frac{\hat{P_Q}}{\hat{P_D}} = \frac{\gamma_Q \mu_Q H}{1-\gamma_Q \mu_Q H}$ (the derivation is in *SI Appendix*). The parameters γ_Q, μ_Q, γ_D, and μ_D are associated with the vertical shapes of vertical motion or QG forcing profiles. As will be seen below, their changes with warming are of secondary importance. The dependence of $\hat{P_D}$ and $\hat{P_Q}$ with T_s is shown in Fig. 3*A*. The amplification parameter α quantifies the diabatic heating feedback on precipitation due to QG adjustments (21). In general, α depends on the horizontal length scale of the disturbance, the background state, and the adiabatic forcings (21, 22), with larger α meaning stronger P under the same F. In the control case, $\alpha = 1.1$, similar to the value found in the case of the 2010 Pakistan extreme precipitation event (22). As T_s increases from the coldest to the warmest case, α increases from 0.6 to 3.5, indicating that the diabatic heating feedback becomes stronger with warming.

Based on Eq. **4**, we can decompose $\delta \ln \hat{P}$ as

$$\begin{aligned}\delta \ln \hat{P} &= \delta \ln \hat{P_D} + \delta \ln(\alpha + 1) \\ &= (\delta \ln \gamma_D + \delta \ln \mu_D + \delta \ln H + \delta \ln \langle F \rangle) + \\ &\quad \alpha(\delta \ln \gamma_Q + \delta \ln \mu_Q + \delta \ln H). \qquad [5]\end{aligned}$$

The terms in Eq. **5** are shown in Fig. 3*C*. The contributions from the changes of vertical shapes are generally small, except that $\alpha \delta \ln \mu_Q$ (reflecting the change of the vertical structure of Q) (*SI Appendix*, Fig. S5) becomes nonnegligible for large T_s. One dominant term in Eq. **5** is $\delta \ln H$, which represents the change of $\hat{P_D}$ due to increased precipitable water with approximately unchanged ω_D. The other dominant term is $\alpha \delta \ln H$, meaning that the thermodynamic effect is amplified by the diabatic heating feedback by α. Comparing Eq. **5** with Eq. **3**, we have $\delta \ln \Omega \approx \alpha(\delta \ln H + \delta \ln \mu_Q)$, stating that the dynamic component of precipitation extremes is mainly due to the increased diabatic heating leading to increased ω_Q, modified by a secondary term associated with the changes in the vertical structure of heating.

The numerical results are summarized in Fig. 4 together with another group of experiments performed as sensitivity tests (*SI Appendix*). $\delta \ln P$ increases about two times faster than $\delta \ln H$, indicating a nearly double CC scaling in these simulations on average. The scatter points are above the linear fit line, consistent with the fact that $\frac{\delta \ln P}{\delta T_s}$ increases as T_s increases (Fig. 3*B*). In

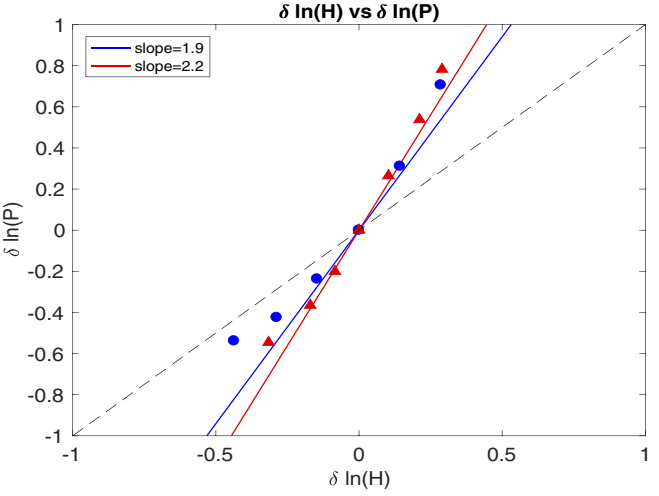

Fig. 4. Changes in extreme precipitation ($\delta \ln P$) vs. changes in column water vapor ($\delta \ln H$) from experiment group 1 (blue circles) and experiment group 2 (red triangles) (*SI Appendix*). The black dashed line is the one-to-one line. Blue and red lines are the linear fit lines to the two experiment groups.

experiment group 2, the CRM is subject to time-constant T and q forcings to better match the CRM background profiles with those of CMIP5 (*SI Appendix*, Figs. S7 and S8). The results of experiment group 2 are qualitatively similar to those of group 1 shown in the text; the diabatic heating feedback is weaker but still significantly contributes to the super-CC sensitivity of extreme precipitation (*SI Appendix*, Fig. S9).

Fig. 5 summarizes the feedbacks in the CQG system and how it amplifies the sensitivity of precipitation extremes to warming. Under the current climate, the adiabatic QG forcing (F) induces vertical motion (ω_D), which on its own, would produce precipitation P_D. The feedback due to the latent heating release on QG ω leads to vertical motion of ω_Q, providing an additional component of precipitation, P_Q. The strength of the feedback is quantified as α, so that the total precipitation is the adiabatic QG component multiplied by $\alpha+1$. In a warmer climate, while there is little change in ω_D (due to the assumed constancy of F here as well as the smallness of the changes in σ), the increased water vapor leads to increasing P_D at the rate $\delta \ln H$. This thermodynamic contribution is further amplified by the diabatic feedback by α and expressed largely as the dynamic contribution. At the same time, the vertical structures of q and Q may change, leading to secondary terms $\delta \ln \gamma_D$, $\delta \ln \gamma_Q$, $\delta \ln \mu_D$, and $\delta \ln \mu_Q$; here, these terms are negative and reduce the magnitude of the positive sensitivity. Because the total diabatic heating feedback α is positive and becomes larger in a warmer climate, the sensitivity of precipitation extremes with surface temperature exceeds CC scaling.

Conclusions and Discussion

We have investigated the sensitivity of precipitation extremes to temperature using the extreme precipitation event of May 2015 in Texas and Oklahoma as an example and studied it with idealized CRM simulations on a small domain under the CQG method. The 2015 event was simulated under different climatic background conditions with varying T_s under the same adiabatic QG forcing. In the control case, under the actual climatic conditions in 2015, the model results reproduce the precipitation in observations reasonably well, while perturbed cases show that the extreme precipitation increases exponentially as T_s increases. The exponential growth rate exceeds CC scaling due to the positive contribution from the dynamic response due to increased large-scale ascent driven by increased diabatic heating. It is approximately equal to the relative changes of atmospheric moisture multiplying a diabatic heating amplification factor α, modified by a secondary term associated with the changes in the vertical structure of heating. While the thermodynamic contribution is nearly constant with warming, the diabatic heating feedback becomes stronger, leading to increasing extreme precipitation sensitivity.

The super-CC scaling for extreme precipitation that we find here is consistent with some observational and GCM modeling studies (10, 12). Our results are strictly for a single event, but we view them as relevant to a larger set of events with a strong convective component as well as strong large-scale PV dynamics. Particularly interesting examples may include precipitation extremes in the subtropics during the summer half-year, including those caused by tropical–extratropical interaction (41), as well as monsoon depressions (42) and similar disturbances. Similar considerations may apply to a wider range of midlatitude precipitation systems accompanied by convection as well, although since the dynamic amplification that we find is greatest for the warmest climates, we might expect it to be smaller for winter storms.

The CQG method allows us to analyze in detail the mechanisms by which the super-CC scaling comes about, providing perspective relevant to interpreting the different extreme precipitation sensitivities found in GCM simulations. Climate models with stronger diabatic heating feedback in simulations of the current climate are likely to produce greater sensitivity of extreme precipitation to climate change, such as has been found for the response of the North Atlantic storm track to warming in a regional model sensitivity study (43). The CQG method could be used to diagnose in more detail the mechanisms leading to different results in different climate models.

A significant limitation of this study is that we assume that the adiabatic QG forcing and the horizontal length scale associated with the disturbance remain constant as climate changes, so that all changes are driven directly by the changing thermodynamic environment. We view this as a reasonable starting point given the greater uncertainty in dynamic compared with thermodynamic components of climate change (30–32, 34). Other factors not considered here include, for instance, the effects of large-scale circulation pattern changes on local regions (44), the possible changes of eddy length scale (45), and the possible changes of frequencies of strong synoptic perturbations (46). All of these factors may also modify the sensitivity of extreme

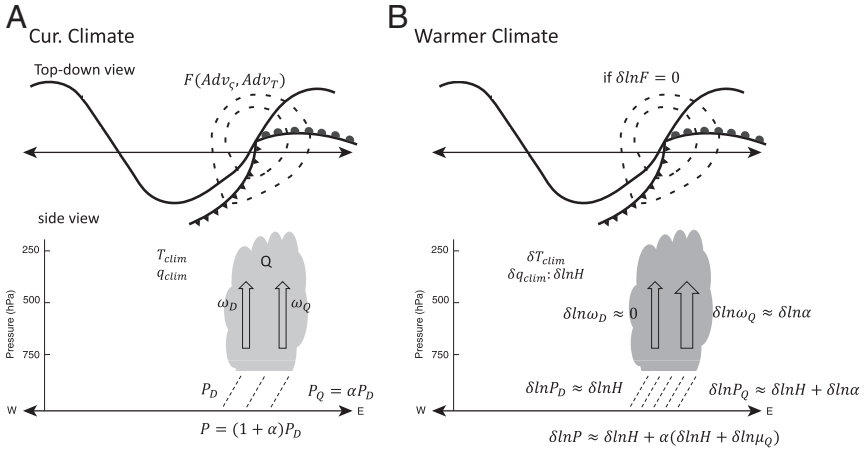

Fig. 5. A schematic of the scaling of precipitation extremes with temperature in a CQG system. *A* is under the current climate. *Upper* shows an upper level synoptic wave, lower level fronts, and a low-pressure center. *Lower* shows the side view of the convecting and precipitating region over the low-pressure center. *B* is in a warmer climate: the fractional changes of vertical motion and precipitation if the large-scale adiabatic QG forcing *F* (and Adv_q) is unchanged. The darker color of the cloud cartoon indicates that the convective system is stronger in a warmer climate.

precipitation. Studies with comprehensive climate models suggest, in fact, that warming may lead to a reduction in the dynamic component of extreme precipitation in the region and season of interest here (11, 45). If so, our results suggest that this reduction is due to these other effects, with dynamic amplification due to increased heating (for a given F and wave number k) still relevant and perhaps dominant in other regions. Efforts to analyze all of these effects more broadly using a hierarchy of numerical models would be valuable.

ACKNOWLEDGMENTS. We thank two anonymous reviewers for their helpful reviews. This research was supported by National Natural Science Foundation of China Grant 41875050 (to J.N.), an AXA Award from the AXA Research Fund (to A.H.S.), and National Science Foundation Grant AGS-1543932 (to S.W.).

1. Trenberth KE (1998) Atmospheric moisture residence times and cycling: Implications for rainfall rates with climate change. *Clim Change* 39:667–694.
2. Allen MR, Ingram WJ (2002) Constraints on future changes in climate and the hydrologic cycle. *Nature* 419:224–232.
3. Held I, Soden B (2006) Robust responses of the hydrological cycle to global warming. *J Clim* 19:5686–5699.
4. Sherwood SC, et al. (2010) Relative humidity changes in a warmer climate. *J Geophys Res* 115:D09104.
5. Kumar S, Merwade V III, Kinter JL, Niyogi D (2013) Evaluation of temperature and precipitation trends and long-term persistence in CMIP5 twentieth-century climate simulations. *J Clim* 26:4168–4185.
6. Alexander LV, et al. (2006) Global observed changes in daily climate extremes of temperature and precipitation. *J Geophys Res* 111:D05109.
7. Westra S, Alexander LV, Zwiers FW (2013) Global increasing trends in annual maximum daily precipitation. *J Clim* 26:3904–3918.
8. Kharin VV, Zwiers FW, Zhang X, Hegerl GC (2007) Changes in temperature and precipitation extremes in the IPCC ensemble of global coupled model simulations. *J Clim* 20:1419–1444.
9. O'Gorman PA, Schneider T (2009) The physical basis for increases in precipitation extremes in simulations of 21st century climate change. *Proc Natl Acad Sci USA* 106:14773–14777.
10. Sugiyama M, Shiogama H, Emori S (2010) Precipitation extreme changes exceeding moisture content increases in MIROC and IPCC climate models. *Proc Natl Acad Sci USA* 107:571–575.
11. Pfahl S, O'Gorman PA, Fischer EM (2017) Understanding the regional pattern of projected future changes in extreme precipitation. *Nat Clim Change* 7:423–428.
12. Shiu CJ, Liu SC, Fu C, Dai A, Sun Y (2012) How much do precipitation extremes change in a warming climate? *Geophys Res Lett* 39:L17707.
13. Ban N, Schmidli J, Schär C (2015) Heavy precipitation in a changing climate: Does short-term summer precipitation increase faster? *Geophys Res Lett* 42:1165–1172.
14. Bao J, Sherwood SC, Alexander LV, Evans JP (2017) Future increases in extreme precipitation exceed observed scaling rates. *Nat Clim Change* 7:128–132.
15. Prein AF, et al. (2016) Precipitation in the euro-cordex 0.11 and 0.44 simulations: High resolution, high benefits? *Clim Dyn* 46:383–412.
16. Lackmann G (2013) The south-central us flood of May 2010: Present and future. *J Clim* 26:4688–4709.
17. Kröner N, et al. (2017) Separating climate change signals into thermodynamic, lapse-rate and circulation effects: Theory and application to the European summer climate. *Clim Dyn* 48:3425–3440.
18. Rasmussen KL, Prein AF, Rasmussen RM, Ikeda K, Liu C (2017) Changes in the convective population and thermodynamic environments in convection-permitting regional climate simulations over the United States. *Clim Dyn*, 10.1007/s00382-017-4000-7.
19. Trapp RJ, Hoogewind KA (2016) The realization of extreme tornadic storm events under pseudo-global warming. *J Clim* 29:5251–5265.
20. Pall P, Allen MP, Stone DA (2007) Testing the Clausius–Clapeyron constraint on changes in extreme precipitation under CO_2 warming. *Clim Dyn* 28:351–363.
21. Nie J, Sobel AH (2016) Modeling the interaction between quasi-geostrophic vertical motion and convection in a single column. *J Atmos Sci* 73:1101–1117.
22. Nie J, Shaevitz DA, Sobel AH (2016) Forcings and feedbacks on convection in the 2010 Pakistan flood: Modeling extreme precipitation with interactive large-scale ascent. *J Adv Model Earth Syst* 8:1055–1072.
23. Sobel AH, Bretherton CS (2000) Modeling tropical precipitation in a single column. *J Clim* 13:4378–4392.
24. Raymond DJ, Zeng X (2005) Modelling tropical atmospheric convection in the context of the weak temperature gradient approximation. *Q J R Meteorol Soc* 131:1301–1320.
25. Kuang Z (2008) Modeling the interaction between cumulus convection and linear waves using a limited domain cloud system resolving model. *J Atmos Sci* 65:576–591.
26. Romps DM (2011) Weak pressure gradient approximation and its analytical solutions. *J Atmos Sci* 69:2835–2845.
27. Muller C, O'Gorman PA, Back L (2011) Intensification of precipitation extremes with warming in a cloud-resolving model. *J Clim* 24:2784–2800.
28. Lackmann GM (2015) Hurricane sandy before 1900 and after 2100. *Bull Am Meteorol Soc* 96:547–560.
29. Stott PA, et al. (2016) Attribution of extreme weather and climate-related events. *Wires Clim Change* 7:23–41.
30. Trenberth KE, Fasullo JT, Shepherd TG (2015) Attribution of climate extreme events. *Nat Clim Change* 5:725–730.
31. Shepherd TG (2016) A common framework for approaches to extreme event attribution. *Curr Clim Change Rep* 2:28–38.
32. Lloyd EA, Oreskes N (2018) Climate change attribution: When is it appropriate to accept new methods? *Earth's Future* 6:311–325.
33. Khairoutdinov MF, Randall DA (2003) Cloud resolving modeling of the arm summer 1997 IOP: Model formulation, results, uncertainties, and sensitivities. *J Atmos Sci* 60:607–625.
34. O'Gorman PA (2015) Precipitation extremes under climate change. *Curr Clim Change Rep* 1:49–59.
35. Dee DP, coauthors (2011) The era-interim reanalysis: Configuration and performance of the data assimilation system. *Q J R Meteorol Soc* 137:553–597.
36. Chen M, et al. (2008) Assessing objective techniques for gauge-based analyses of global daily precipitation. *J Geophys Res* 113:D04110.
37. Shepherd TG (2014) Atmospheric circulation as a source of uncertainty in climate change projections. *Nat Geosci* 7:703–708.
38. Huffman GJ, et al. (2001) Global precipitation at one-degree daily resolution from multisatellite observations. *J Hydrometeor* 2:36–50.
39. Prein AF, coauthors (2015) A review on regional convection-permitting climate modeling: Demonstrations, prospects, and challenges. *Rev Geophys* 53:323–361.
40. O'Gorman PA, Muller J (2010) How closely do changes in surface and column water vapor follow Clausius-Clapeyron scaling in climate change simulations? *Environ Res Lett* 5:025207.
41. Pascale S, Bordoni S (2016) Tropical and extratropical controls of gulf of California surges and summertime precipitation over the southwestern United States. *Mon Weather Rev* 144:2695–2718.
42. Hurley JV, Boos WR (2014) A global climatology of monsoon low-pressure systems. *Q J R Meteorol Soc* 141:1049–1064.
43. Willison J, Robinson WA, Lackmann GM (2015) North Atlantic storm-track sensitivity to warming increases with model resolution. *J Clim* 28:4513–4524.
44. Lu J, et al. (2014) The robust dynamical contribution to precipitation extremes in idealized warming simulations across model resolutions. *Geophys Res Lett* 41:2971–2978.
45. Tandon NF, Zhang X, Sobel AH (2018) Understanding the dynamics of future changes in extreme precipitation intensity. *Geophys Res Lett* 45:2870–2878.
46. Trapp RJ, Diffenbaugh NS, Gluhovsky A (2009) Transient response of severe thunderstorm forcing to elevated greenhouse gas concentrations. *Geophys Res Lett* 36:L01703.